JOURNAL OF PROPULSION AND POWER
Vol. 19, No. 5, September–October 2003

Two-Dimensional Compressible Non-Acoustic Modeling of Stirling Machine-Type Components

Roy C. Tew Jr.*
NASA John H. Glenn Research Center at Lewis Field, Cleveland, Ohio 44135-3191
and
Mounir B. Ibrahim†
Cleveland State University, Cleveland, Ohio 44115-2425

Starting with an existing two-dimensional incompressible flow computer code, a two-dimensional code was developed for modeling enclosed gas volumes with oscillating boundaries. The incompressible code was modified to use compressible nonacoustic Navier–Stokes equations. The devices modeled have low Mach numbers and are sufficiently small that the time required for acoustics to propagate across the interiors is small compared to the cycle period. Therefore, acoustics were excluded to minimize computing time. The compressible nonacoustic assumptions are discussed. The governing equations are presented in transport equation format. The numerical methods are briefly described. Code predictions are compared with experimental data. Compressible nonacoustic predictions of gas spring losses agreed well with 10-rpm test data, and ~50- and 500-rpm calculated and experimental pressure–volume diagrams agreed well. For a heat-exchanger/piston-cylinder test rig, calculations of heat exchanger heat fluxes at various axial locations over the cycle agreed well qualitatively with the data, but quantitative agreement was not good.

Nomenclature

c_p = specific heat at constant pressure
D_h = hydraulic diameter, four times flow area/wetted perimeter
$\bar{D}$ = viscous force vector
F = functional representation of general equation of state (4)
$\bar{f}$ = mass force vector (due to gravity, for example)
P = mean spatial pressure
P_a = amplitude of mean spatial pressure
P_0 = arithmetic mean of maximum and mininum mean spatial pressures
p = static pressure
Q = density of continuously distributed heat sources
q_m = entropy source due to nonzero mass sources
R = gas constant
r_v = volume ratio (maximum/minimum)
S = source term
s = entropy per unit mass
T = temperature
$\bar{\bar{T}}_{ST}$ = stress tensor
$\bar{\bar{T}}_{ST,S}$ = source part of stress tensor
t = time
U = axial, x direction, velocity
$\bar{u}$ = velocity vector, $\bar{i}U + \bar{j}V$
V = radial, r direction, velocity or volume
V_0 = arithmetic mean of maximum and minimum volumes
$\dot{W}_{loss}$ = nondimensional work or hysteresis loss
$\bar{w}$ = rate of momentum change because of mass sources, $\xi\rho\bar{u}$
Γ_ϕ = diffusion coefficient
γ = ratio of specific heats of fluid
λ = molecular thermal conductivity
μ = absolute viscosity
ξ = mass source strength per unit mass
ρ = density, fluid mass per unit volume
ρ_0 = arithmetic mean of maximum and minimum densities
ϕ = transport quantity per unit mass
ω = angular velocity, rad/s

Received 21 May 2002; revision received 19 March 2003; accepted for publication 5 May 2003.

*Research Engineer, Thermo-Mechanical Systems Branch, Mail Stop 301-2, 21000 Brookpark Road; Roy.C.Tew@nasa.gov. Member AIAA.
†Professor, Fenn College of Engineering, Mechanical Engineering Department, 1960 East 24th Street; m.ibrahim@csuohio.edu. Member Associate Fellow AIAA.

Introduction

Background

THE work reported here has supported Stirling engine development underway for more than 25 years.[1–5] Two one-dimensional Stirling design codes have been used.[6,7] Experience indicates that initial engine power is typically 10–20% less than one-dimensional design code predictions. The one-dimensional codes assume uniform axial flow and, thus, are deficient in modeling interfaces where area changes occur (and other approximations are required). Past comparisons of one-dimensional design code predictions[8] have shown rough overall performance agreement but significant differences in individual losses.

The multidimensional Stirling code development reported here began as a strategy to improve characterization of thermodynamic losses.[3] Makhamov and Ingham[9] indicate a two-dimensional code has been used to aid Stirling engine design at the Stirling Engine Laboratory at the Physical-Technical Institute in Tashkent, Uzbekistan.

Objective of the Work and Work Reported

The immediate goal of the two-dimensional code development reported here was a time-efficient code for study of Stirling type cylinder heat transfer/power (hysteresis) losses (see Tew[10]). A long-range goal was to provide the basis for development of a two-dimensional model of a complete Stirling engine.

Therefore, starting with an existing two-dimensional incompressible flow code, CAST,[11] a two-dimensional code was developed for modeling enclosed volumes of gas with oscillating boundaries. This incompressible code was modified to use compressible nonacoustic Navier–Stokes equations.[12] The devices modeled have low Mach numbers, but oscillating gas volumes, and are sufficiently small that

the time required for acoustics to propagate across them is small compared to the cycle period. Therefore, acoustics were excluded to minimize computing time. The compressible nonacoustic assumptions are discussed. The governing equations are presented in transport equation format. The numerical methods are briefly described. Code predictions are compared with test data.

Compressible Nonacoustic Flow

Assumptions

Fedorchenko[12] discusses a number of subsonic initial-boundary-value problems that cannot be solved using the classical theory of incompressible fluid motion, which involves the equation $\nabla \cdot \bar{\boldsymbol{u}} = 0$. Among these problems are 1) closed-volume flows initiated by blowing or suction through permeable walls, 2) closed-volume flows initiated by a moving piston, 3) flows with continuously distributed mass sources, and 4) viscous flows with substantial heat fluxes. Fedorchenko notes that use of the most general theory of compressible fluid flow may not be best in such cases because of difficulties in accurately resolving complex acoustic phenomena and in assigning proper boundary conditions.

Fedorchenko[12] proposes a nonlocal mathematical model where $\nabla \cdot \bar{\boldsymbol{u}} \neq 0$, in general, for simulation of unsteady subsonic flows in a bounded domain with continuously distributed mass, momentum, and entropy sources, which also accounts for effects of viscosity and conductivity when necessary. The exclusion of sound waves is an important feature of the model.

The most general form of Fedorchenko's[12] compressible nonacoustic system of equations for simulation of unsteady, subsonic, heat-conducting viscous flows are as follows.

Momentum:

$$\frac{\partial(\rho\bar{\boldsymbol{u}})}{\partial t} + \nabla \cdot \rho\bar{\boldsymbol{u}}\bar{\boldsymbol{u}} + \nabla p = \rho\bar{\boldsymbol{f}} + \bar{w} + \bar{\boldsymbol{D}} \tag{1}$$

Continuity:

$$\frac{\partial\rho}{\partial t} + \nabla \cdot \rho\bar{\boldsymbol{u}} = \xi\rho \tag{2}$$

Energy:

$$\frac{\partial s}{\partial t} + \bar{u} \cdot \nabla s = \frac{R}{P}[\nabla \cdot \lambda\nabla T + Q] + q_m \tag{3}$$

State:

$$F(s, P, \rho) = 0 \tag{4}$$

Several less common variables used in these equations are defined in the Nomenclature.

When $\nabla\mu = 0$ (as for constant viscosity problems) then the viscous force vector is

$$\bar{\boldsymbol{D}} = \mu\Delta\bar{\boldsymbol{u}} + \tfrac{1}{3}\mu\nabla(\nabla \cdot \bar{\boldsymbol{u}}) \tag{5}$$

Note that the energy equation is written in terms of entropy s rather than in terms of internal energy, enthalpy, or temperature.

Simplifications in the Navier–Stokes equations used to eliminate acoustics and arrive at the preceding system of equations were 1) pressure at time t and position $\bar{r}$ is split into a mean spatial pressure level that varies with time and a Δ (pressure) that varies with position and time,

$$p(\bar{r}, t) = P(t) + \Delta p(\bar{r}, t) \tag{6}$$

2) the pressure, $P(t)$ appearing in the equations of energy and state is the mean spatial pressure that varies only with time. Therefore, from the ideal gas equation of state

$$\rho = P(t)/RT(\bar{r}, t) \tag{7}$$

Thus, density is a function of mean spatial pressure level and the temperature field (and is independent of the spatial pressure drop).

Simplification of Equations for the Stirling Problem

Because, for the Stirling piston/cylinder problem, there are no distributed mass or heat sources and the gravity force is not of interest, the variables $\bar{\boldsymbol{f}}$, $\bar{w}$, ξ, Q, and q_m in Eqs. (1–3) are all zero. Also the ideal gas equation of state is sufficiently accurate for the helium gas used in Stirling engines of interest. Therefore, Eqs. (1–4) reduce to the following set:

$$\frac{\partial(\rho\bar{\boldsymbol{u}})}{\partial t} + \nabla \cdot \rho\bar{\boldsymbol{u}}\bar{\boldsymbol{u}} + \nabla p = \bar{\boldsymbol{D}} \tag{8}$$

$$\frac{\partial\rho}{\partial t} + \nabla \cdot \rho\bar{\boldsymbol{u}} = 0 \tag{9}$$

$$\frac{\partial s}{\partial t} + \bar{\boldsymbol{u}} \cdot \nabla s = \frac{R}{P}[\nabla \cdot \lambda\nabla T] \tag{10}$$

$$\rho = \frac{P}{RT} \tag{11}$$

CAST and Modified CAST Codes

The incompressible flow CAST code was originally acquired from Peric and Scheuerer.[11] Many CAST numerical techniques are also discussed by Ferziger and Peric.[13] Changes made to CAST to develop the modified CAST compressible nonacoustic code are documented by Tew.[10]

Transport Equation Format

The CAST solution technique is based on a transport equation formulation of the governing equations. The coordinate-free general transport equation used, with terms categorized below, is:

$$\frac{\partial(\rho\phi)}{\partial t} + \nabla \cdot \left(\rho\bar{u}\phi - \Gamma_\phi\nabla\phi\right) = S_\phi \tag{12}$$

Time rate of storage — convection — diffusion — source

Transport quantities, exchange coefficients, and source terms for the continuity, momentum, and energy equations of modified CAST are shown in Table 1. The energy equation is in enthalpy format, rather than the entropy format used by Fedorchenko.[12] Turbulence model kinetic energy and dissipation rate equations are defined by Tew.[10]

Numerical (Finite Volume) Methods

Modified CAST numerical methods are almost the same as those of CAST.[11] An exception is use of Leibniz's rule (see Ref. 13) to account for the moving piston. Details of the modifications to the finite volume versions of the governing equations are discussed by Tew.[10] The modifications included accounting for the nonzero $\nabla \cdot \bar{\boldsymbol{u}}$ terms, adding the time derivative of the mean-spatial pressure to the energy equation source term, and using mean-spatial pressure in the ideal gas equation. The spatial pressure drop still appears in the momentum equations to help determine the velocity field. Because the density is not affected by spatial pressure variation, the incompressible SIMPLE algorithm[14] still applies.

The governing equations are solved with a conservative finite volume method.[14] The basic approach is two fold. 1) Discretize the solution domain by subdividing it into small axisymmetric (or rectangular) control volumes and locate the numerical grid points in the center of the control volumes. 2) Discretize the transport equations.

Discretization is done by formally integrating the single terms in the equations over a control volume. Application of Leibniz's rule

Table 1 General transport equation; transported quantities, exchange coefficients, and source terms for continuity, energy, and momentum equations

Equation	Transport quantity/vol.	Exchange coefficient	Source term
Continuity	ρ (mass/vol.)	0	0
Momentum	$\rho\bar{\boldsymbol{u}}$ (momentum/vol)	μ	$\nabla \cdot \overline{\overline{T}}_{ST,S}$
Energy	ρh (enthalpy/vol.)	$\lambda/c_p = \mu/Pr$	dP/dt

and Gauss's theorem yields an integro–differential equation relating the net increase in the transported quantity per unit time to the convective and diffusive fluxes across the control volume boundaries and the source/sink terms within the control volume. This practice leads to a conservative method because boundary fluxes leaving one control volume through its right boundary enter the neighboring control volume through its left boundary. Because this principle applies to all control volume faces, the scheme becomes overall conservative. The approach is described by Peric and Scheuerer[11] and Tew[10] in more detail.

CAST Comparisons to Data and Another Computation

Recktenwald[15] Computations and Kornhauser[18] Experimental Data

Recktenwald[15] computed heat transfer between the cylinder walls and gas of a reciprocating compressor. A compressor cylinder contains intake and discharge valves, unlike Stirling engine cylinders. Recktenwald used two-dimensional, unsteady, compressible equations (acoustics included) to simulate the compressor. To validate his computer code, he simulated a gas spring for comparison with data generated by Kornhauser and Smith.[16,17] A schematic of the Kornhauser and Smith gas spring test rig is shown in Fig. 1. The comparison between data and experiment was based solely on experimental and simulated values of nondimensional hysteresis loss over the gas spring operating range. A gas spring is a piston/cylinder, which has no flow to or from the enclosed cylinder volume. Kornhauser[18] reported further details of these experiments. He also reported on tests made with a modification of the gas spring test rig (Fig. 2), to include a heat exchanger mounted on top of the cylinder, such that flow could continuously pass between the cylinder and the heat exchanger as the piston expanded and compressed the gas. This two-space test rig operated more like a Stirling machine cylinder than either a gas spring or a compressor.

Kornhauser's gas spring data[18] were also used as a basis for validation of the two-dimensional modified CAST code. Modified CAST's calculated hysteresis losses were compared with Kornhauser's[18] experimental and Recktenwald's[15] calculated values, over a range of gas spring operation. Also, because Recktenwald published plots of calculated gas spring velocity vectors and temperature contours, these were compared with similar modified CAST results for one operating point. Thus Recktenwald's compressible-acoustic calculations were compared to modified CAST's compressible nonacoustic calculations. Comparison of the two sets of temperature contours over the cycle for a 10-rpm gas spring showed excellent agreement. Agreement between velocities also appeared to be very good, although due to some differences in the velocity vector plots, only a qualitative comparison could be made. These two-dimensional comparisons are shown in Ref. 10.

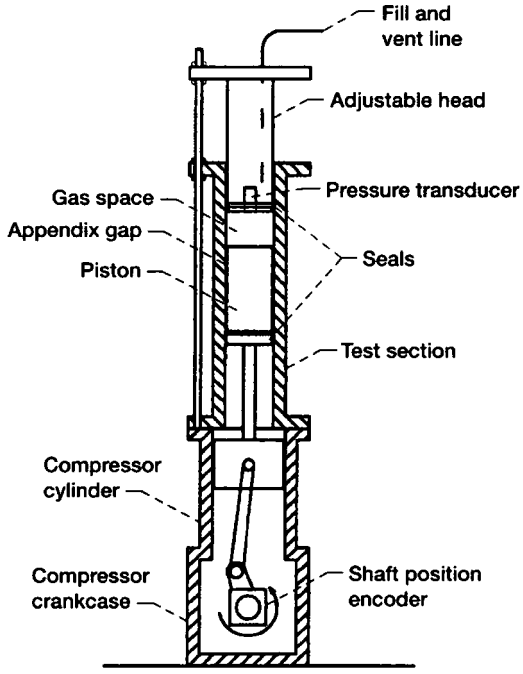

Fig. 1 Kornhauser's and Smith's[16,17] closed-cylinder (gas spring) test rig.

Table 2 Gas spring dimensions

Physical quantity	Value
Cylinder bore (diameter) D	50.80 mm (2 in.)
Piston stroke S	76.2 mm (3 in.)
Volume ratio r_v	2.0

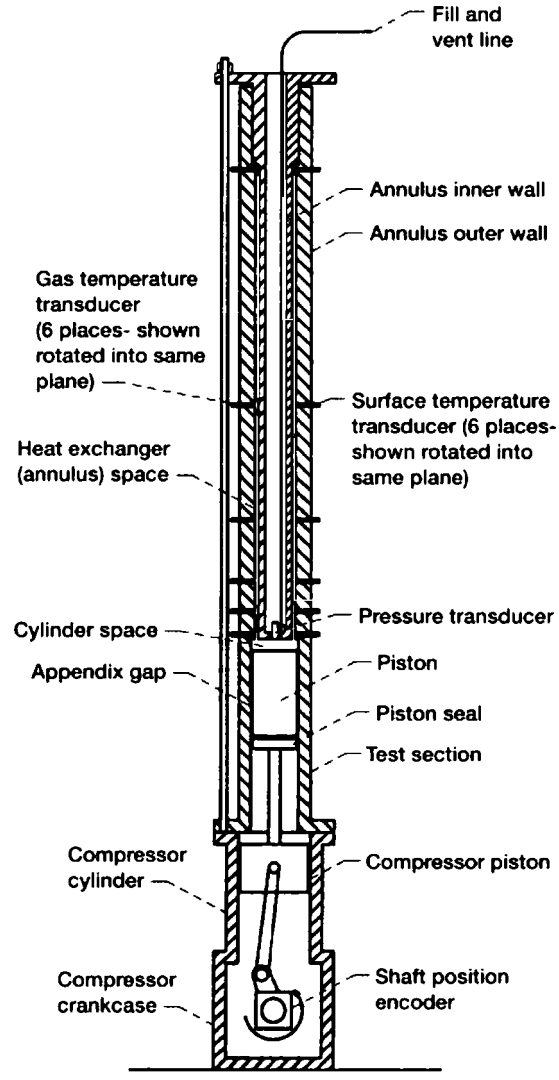

Fig. 2 Kornhauser's[18] two-space (cylinder plus heat exchanger) test rig.

Gas Spring and Two-Space Test Rig Dimensions

The internal dimensions of Kornhauser's test rigs[18] are shown in Tables 2 and 3. Because of a CAST limitation, a slight change was made in the two-space test-rig simulated heat-exchanger geometry. In CAST/modified CAST a grid is generated for the envelope of maximum length and radius (for axisymmetric problems). A volume such as that within the inner radius of the heat exchanger is excluded from the calculations by insertion of a numerical "obstacle." A second obstacle would be needed to fill the small volume between the outer radius of the annular heat exchanger and radius of the cylinder. (One must look closely to see this volume in Fig. 2.) However, CAST can implement only one obstacle.

Table 3 Two-space test-rig dimensions: physical and simulated

Physical quantity	Physical value	Simulation value
Cylinder bore, mm (in.)	50.80 (2)	50.80 (2)
Piston stroke, mm (in.)	76.20 (3)	76.20 (3)
Volume ratio	2.0	2.0
Annulus o.d., mm (in.)	44.5 (1.75)	50.80 (2)
Annulus i.d., mm (in.)	39.4 (1.55)	46.4 (1.83)
Annulus gap, mm (in.)	2.5 (0.10)	2.2 (0.09)
Annulus length, mm (in.)	445 (17.5)	445 (17.5)
Minimum piston/head clearance, mm (in.)	2.9 (0.11)	2.9 (0.11)

Therefore the modeled heat exchanger, physically mounted on top of the cylinder, was moved slightly outward so that the outer wall coincided with the cylinder wall; the heat-exchanger volume was maintained the same to maintain the same volume ratio. Physical and simulated dimensions are shown in Table 3. (It was later estimated that the small geometry change tended to reduce the difference between test and calculated results.) Further code modification was considered to solve this problem. However, since completion of this study, development of multidimensional Stirling models has proceeded via a commercial computational fluid dynamics (CFD) code that does not have CAST's geometry limitation.

Both test rigs used helium gas with walls at a constant temperature of ~294 K (~21°C, 70°F or room temperature).

Computational Grids/Time Steps and Experimental Sources of Error

Double-precision computations were required to achieve convergence of the modified CAST models. The residual's convergence criterion was 0.0001. Minimization of numerical errors was addressed by testing the models with various grid and time step sizes to approach solutions independent of grid and time step size. One practical limitation was that the study was done via an available 150-MHz desktop computer. A few comparison runs were made on the Ohio Supercomputer Center's CRAY computer.

Two subsections to follow on experimental data processing and sources of error are summaries of information from Kornhauser.[18] However, no error analysis was reported that would allow error bars to be shown on the data used in this report.

Gas Spring Model Time Step and Spatial Grid Selection

Recktenwald[15] determined, in simulations of Kornhauser's gas spring,[18] that 17 × 12 grids (axial and radial directions, respectively) with 120 time steps/cycle and 43 × 30 grids with 180 time steps/cycle gave approximately the same results for overall cycle work, heat transfer, and other variables. Therefore, he used 17 × 12 grids with 120 time steps/cycle for most runs, but 43 × 30 grids with 180 times steps/cycle to make field plots of the velocities, temperatures, etc.

Results similar to Recktenwald's[15] were obtained via grid independence and time step studies using the modified CAST code. The modified CAST computations discussed later were made using 18 × 12 grids with 120 time steps/cycle or, when it was desired to make field plots of the velocities and temperatures, 42 × 30 grids with 200 time steps/cycle.

Two-Space Model Time Step and Spatial Grid Selection

For the gas spring simulation, an 18 × 12 grid with 120 time steps/cycle gave adequate results compared to use of 42 × 30 grids and 200 time steps/cycle (for 10 rpm, 193-kPa mean pressure). Thus, an 18 × 12 grid was used to start planning the grid for the cylinder portion of the two-space experiment. Then, eight radial grids were chosen for the heat exchanger. In the cylinder, these 8 radial grids were added to the 12 radial grids previously used in the cylinder. This, then, gave a total of 18 axial × 20 radial cylinder grids (more dense radial grids than for the gas spring).

In the heat exchanger, it would be convenient to have uniform axial grids to simplify heat flux calculations at the entrance, end, and at 1/16, 1/8, 1/4, and 1/2 of the heat exchanger length from the entrance. These were positions where temperatures and heat fluxes were measured. Therefore, initially, a rather coarse, uniform, 16 grids were used along the axis of the heat exchanger. Thus, this initial grid had 16 axial x 8 radial grids inside the heat exchanger annulus and 18 × 20 grids in the cylinder for a total of 34 axial × 20 radial grids. There were 120 time steps/cycle chosen, initially, as used with the 18 × 12 gas spring grid.

With this 34 × 20 grid, average grid densities in regions of the computational domain were as follows. In the heat exchanger, axial grid density was a coarse one grid every 2.78 cm; radial average grid density was ~36 grids/cm. In the cylinder, radial average grid density inside the heat-exchanger inner radius was ~5 grids/cm; between the inner and outer heat-exchanger radii, radial grid density was the same as the heat exchanger, ~36 grids/cm. Cylinder axial grid densities were 62 grids/cm at top-dead-center (TDC) and ~2.3 grids/cm at bottom-dead-center. The coarseness and uniformity of the initial axial heat-exchanger grid was considered a possible problem.

For experimentation with the number of axial grids, cylinder radial grids were fixed at 20, with 8 in the heat-exchanger and 12 in the non-heat-exchanger region. Axial grids in the heat exchanger were increased from 16 to as large as 128 (factor of 8), using both uniform and non-uniform grids. In the cylinder, in addition to the earlier used 18 axial grids, several runs were made with only 8 axial grids. The already small grid size, when compressed at TDC, seemed to argue against going to a larger number of cylinder axial grids. Further increases in the number of radial grids in the annular heat exchanger would have been desirable. This was not done due to desktop computer and time limitations. This same problem has more recently been modeled by Ibrahim, et al.,[19] using the CFD–ACE commerical code (which does not exclude acoustic phenomena) with up to 20 radial grids in the annular heat exchanger. These CFD–ACE computations did not improve upon the earlier modified CAST computations (reported here), in achieving agreement with Kornhauser's heat exchanger heat flux data.[18]

Gas Spring Test Rig: Experimental Data Processing and Sources of Error[18]

The summarized information in this and the following section was taken from Kornhauser.[18] Three full cycles of pressure–volume data were collected for each run. Of these, only one was used for analysis. The remaining data were used to check the level of cycle-to-cycle variations.

The cyclic lost work (hysteresis loss) was calculated by trapezoidal rule integration of $p\,dV$. Comparison of lost work calculated for adjacent cycles showed a variation that never exceeded 0.18% for any run and was generally less than 0.01%.

Instantaneous space-averaged heat transfer and mixed mean gas temperature were calculated from pressure, volume, and time. Work was calculated directly from pressure and volume; heat transfer rate was calculated from work, internal energy, time, and the first law of thermodynamics.

Kornhauser[18] found that helium gas was accurately represented by the ideal gas equation of state. He also found that the appendix gap volume, the small annular clearance volume between the piston and the cylinder wall, began to have a significant effect on the results for volume ratios greater than 2.0 (volume ratio of 2.0, for the experimental runs used here).

According to Kornhauser,[18] pressure transducer inaccuracies made temperature calculations unreliable at the lowest pressure, near isothermal, runs. The transducers had uncertainties of 0.59 (0.086) and 1.8 kPa (0.26 psi) for low- and high-range transducers, respectively. This corresponded to temperature errors of 1.8 and 1.0 K, respectively, for the lowest mean pressure. Because the most nearly isothermal runs had temperature swings as low as 1.7 K, the temperature errors were large enough to make data from these runs unreliable. For higher pressure and "less isothermal" runs, accuracy was adequate. For the highest pressure, largest temperature swing case, there was a temperature uncertainty of about 0.3 K for a gas temperature swing over the cycle of 230 K. The results of the most

nearly isothermal runs were used only for loss, pressure phase, and pressure magnitude measurements. The lowest temperature swing of any run for which heat transfer results were reported was 16 K.

Two-Space Test Rig: Experimental Data Processing and Sources of Error[18]

Cyclic lost work and instantaneous space-averaged heat transfer, were calculated by Kornhauser[18] the same way as for the gas spring apparatus. Annulus gas–wall heat transfer was calculated from surface temperature test data by modeling the wall as a semi-infinite solid subjected to sinusoidal surface temperature variations. The surface temperature was Fourier decomposed into sinusoidal components, and heat transfer corresponding to each component was calculated. Components were recombined to get total heat transfer. This Fourier procedure could be used only for the ac heat transfer component. The dc component could not be calculated from these data because by the time cyclic steady state was attained for the gas, the dc temperature wave had penetrated the substrate. An approximate value for the dc heat transfer was calculated using cyclic-average values of wall temperature for all cycles beginning with the apparatus startup. The wall was modeled as a semi-infinite solid subjected to a step change in surface heat flux. Approximate dc heat transfer was calculated from the change in cyclic-average wall temperature at startup, when the substrate could still be considered semi-infinte.

Cylinder heat transfer was calculated by subtracting the heat transfer calculated from heat exchanger surface resistance temperature detector (RTD) measurements from total heat transfer calculated from pressure–volume measurements. To do this, it was necessary to interpolate heat fluxes measured at each RTD location to find the heat flux at each point in the heat exchanger.

Center gas temperature in the heat exchanger was measured directly. Kornhauser's[18] mixed mean gas temperature in the cylinder space was calculated using both the heat-exchanger temperature measurements and pressure–volume measurements.

The error sources present for the gas spring experiments apply for the two-space experiments as well. In addition, there were error sources unique to the two-space experiments.

Kornhauser's[18] surface heat flux calculations were based on the assumption that the transducer could be modeled as an infinitely thin sensor mounted on an infinitely thick, one-dimensional homogeneous substrate. The assumption of a thin sensor was thought to be quite good. The assumption of a semi-infinite one-dimensional wall led to errors in surface heat flux calculation such that only data taken at 50 rpm and above were felt to be reliable by Kornhauser.

Probably the most important sources of error were in calculation of temperature and, to a lesser extent, heat transfer in the cylinder space. Because of the complex oscillating pressure/oscillating flow conditions, the temperature profile across the heat exchanger was not known. Because of the small size of the annulus, temperature could be measured only at or near the centerline, according to Kornhauser.[18] (A 10 × microscope was used to investigate deviations from the centerline position.) In calculating cylinder-space temperature, gas mass in the heat exchanger was calculated on the assumption that the centerline temperature was representative of the mean cross-sectional temperature. This could result in serious miscalculation of the mass and, thus, the temperature in the cylinder space. In addition to having only a centerline temperature measurement, the temperatures were interpolated between the measurement locations along the length of the heat exchanger. This provided another possible error source.

Results: Computations Virsus Test Data

Gas Spring Hysteresis Losses

For a gas spring, hysteresis loss is work dissipated by the spring per cycle at steady operating conditions; it is also equal to the heat generated in and transferred out of the spring. A good way to compare computational and measured hysteresis losses is via plots of dimensionless work as a function of oscillating-flow Peclet number (see Ref. 18). Dimensionless work and oscillating-flow Peclet numbers are defined, respectively, as follows:

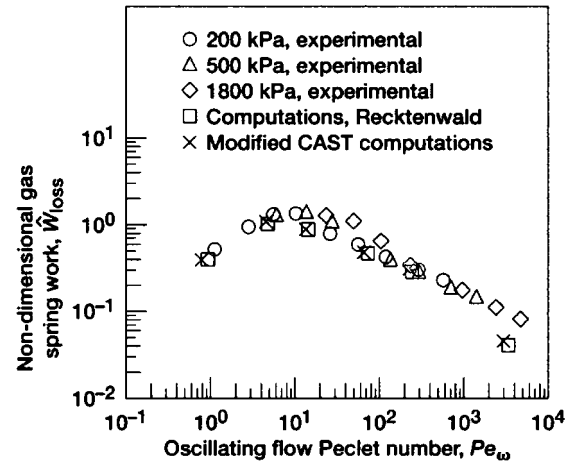

Fig. 3 Gas spring losses: modified CAST, recktenwald[15] calculations, and Kornhauser's[18] measurements.

$$\hat{W}_{\text{loss}} = \oint P\,\mathrm{d}V \Big/ P_0 V_0 \left(\frac{P_a}{P_0}\right)^2 \left(\frac{\gamma - 1}{\gamma}\right) \tag{13}$$

$$Pe_\omega = \frac{\rho_0 c_p \omega D_h^2}{4\lambda} \tag{14}$$

Recktenwald[15] had previously plotted his calculated dimensionless losses on a plot of Kornhauser's data.[18] The modified CAST dimensionless losses were superimposed on this plot with the result shown in Fig. 3. Figure 3 shows dimensionless loss as a function of oscillating-flow Peclet number. The modified CAST values were plotted at "uncorrected" Peclet numbers (see Ref. 10) (based on integral average densities). If plotted at the corrected values of the Peclet numbers (see Ref. 10), that is, based on arithmetic mean densities, as by Recktenwald,[15] they would be shifted slightly to the right and would fall on Recktenwald's values.

Five of the six pairs (modified CAST and Recktenwald values[15]) of calculated dimensionless losses agree well with Kornhauser's data.[18] The one pair of calculated points that did not agree with the data is shown at the highest Peclet number and corresponds to a 1000-rpm, 1465-kPa gas spring operating condition. Recktenwald[15] discusses several plausible explanations for disagreement at high Peclet number Pe_ω: 1) At large Peclet number Pe_ω the gas spring approaches adiabatic behavior and hysteresis losses become small, and so a small error will have large consequences. 2) Wall heat transfer may be underpredicted by the calculations (both sets) due to assumptions of constant thermal conductivity corresponding to 300 K, while temperatures varied between 250 and 400 K for this near adiabatic point. 3) Systematic error in the experimental results is a possibility.

In the data midrange, near $Pe_\omega = 10$, where higher and lower data curves occur, the computations agree with the lower curve. Kornhauser[18] found the higher and lower curves were related to differences between data taken at high pressure/low-speed (higher) and those taken at low pressure/high speed (lower). He concluded there was some other dimensionless parameter needed to resolve the data in this range. His experiment also showed that adding fins within the gas spring clearance volume suppressed the difference in losses, that is, between high-pressure/low-speed and low-pressure/high-speed losses. See Kornhauser[18] for more discussion.

Comparison of modified CAST and experimental pressure–volume (P–V) diagrams are shown in Figs. 4 and 5 for ~49 and 496 rpm, respectively. Agreement is very good.

Two-Space Test Rig Data and Calculation Comparisons

Figures 6 and 7 show experimental heat-exchanger heat fluxes and annulus center-to-wall temperature difference for Kornhauser's[18] two-space rig. Figures 8 and 9 show corresponding modified CAST

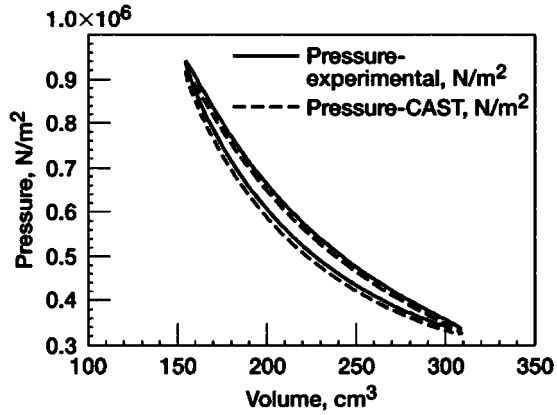

Fig. 4 Gas spring experimental[18] and modified CAST P–V diagrams for 48.6 rpm, 555.7-kPa mean pressure.

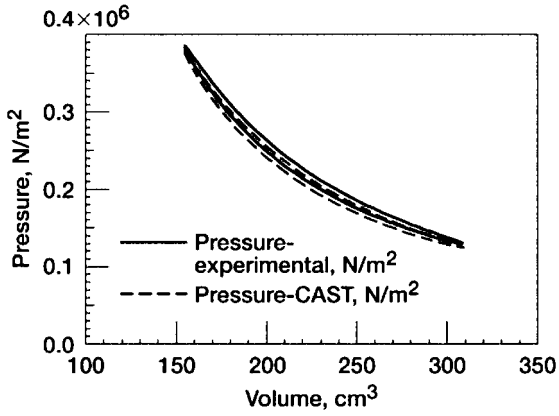

Fig. 5 Gas spring experimental[18] and modified CAST P–V diagrams for 495.8 rpm, 223.3-kPa mean pressure.

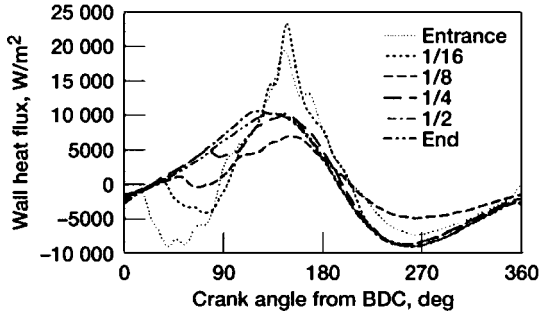

Fig. 6 Measured[18] two-space test-rig heat-exchanger heat fluxes for 201.7 rpm, 1.008-MPa mean pressure.

results for comparison with Figs. 6 and 7. Experimental and calculated heat transfer have different signs due to differences in definition of the positive heat transfer direction.

Figures 6 and 8 show that peak experimental heat flux near the entrance is 4000–5000 W/m^2 less (~17%) than the calculated value; near the end, the peak experimental value is ~9000 W/m^2 less (~45%) than the calculated value. Therefore, even though the qualitative variations in heat transfer look similar in the experimental and calculated plots, quantitative agreement is not good.

Comparison of the annulus center to wall temperature differences in Figs. 7 and 9 show that the calculated temperature differences are smaller that the experimental values. This is consistent with the calculated heat fluxes being larger than the experimental values.

Two-dimensional plots of the Modified CAST calculated temperatures, velocities, pressures, etc., are given in Ref. 10. However, there are no experimental values available for comparison.

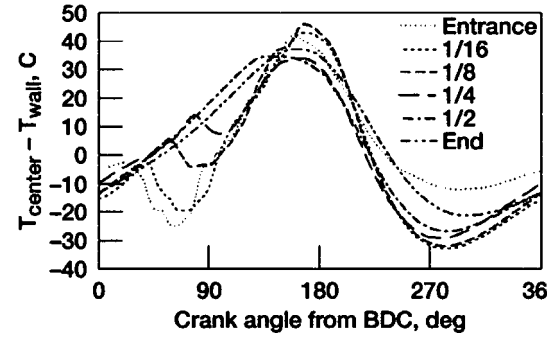

Fig. 7 Measured[18] two-space test-rig heat-exchanger temperature differences for 201.7 rpm, 1.008-MPa mean pressure.

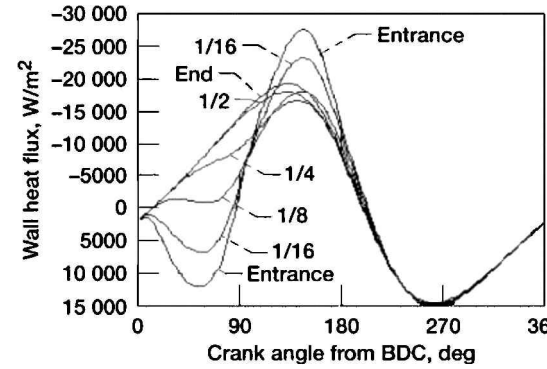

Fig. 8 Modified CAST two-space test-rig heat-exchanger heat fluxes for 201.7 rpm, 1.008-MPa mean pressure.

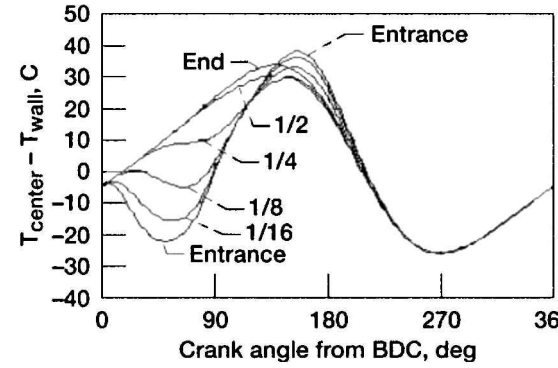

Fig. 9 Modified CAST two-space test-rig heat-exchanger temperature differences for 201.7 rpm, 1.008-MPa mean pressure.

Laminar Versus Turbulent Flow

Laminar Versus Turbulent Flow in Kornhauser Gas Spring[18] at High Speed

Recktenwald[15] assumed that at 500 rpm the flow inside the gas spring was turbulent. His assumption was based on the following reasoning. He calculated that the Reynolds number, based on mean piston speed, gas spring geometry, and mean helium properties, was 1026. He thought it reasonable to assume that agitation by the piston and the large volume changes are sufficient to induce large-scale, unstable motions that give rise to turbulence. Recktenwald[15] used the Morel–Mansour compressible form of the k–ε turbulence model.[20]

Tew[10] showed that modified CAST, assuming laminar flow, gave approximately the same dimensionless losses as Recktenwald's[15] turbulent calculations, for both 500 and 1000 rpm. Also, when the 1000-rpm simulation was repeated with modified CAST, using the Launder–Spalding incompressible k–ε turbulence model,[21] there was very little change in the results. Later, for two-space test-rig turbulent flow simulations, both the Launder–Spalding incompressible

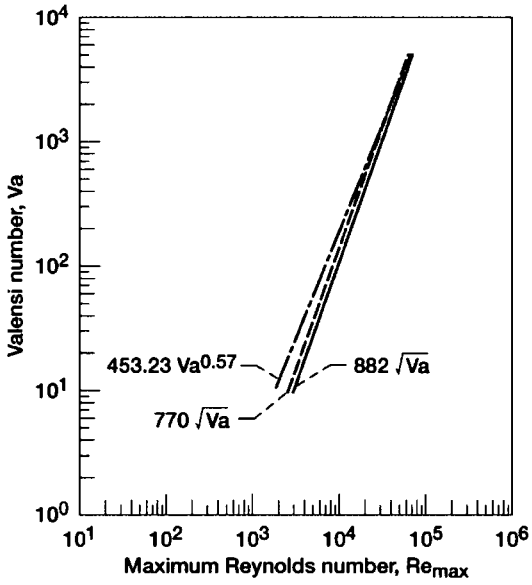

Fig. 10 Always-laminar/sometimes-turbulent regions of oscillating pipe flow[27]: labels are criteria of different researchers.

and the Morel–Mansour compressible forms of the k–ε turbulence models were used in modified CAST; differences in the results obtained using the two different forms of the turbulence model were very small. Agreement of the turbulent and laminar calculations for these oscillating-flow simulations could possibly be due to the tendency of k–ε turbulence models to dissipate turbulence too rapidly under these conditions. For example, Koehler et al.[22] found that a low Reynolds number k–ε model dissipated the turbulence in a turbulent slug entering a pipe during oscillating flow much too quickly compared to experimental data.

It is also possible that the maximum Reynolds number was not large enough at these oscillating-flow conditions to generate turbulence. Experiments with oscillating flow in pipes have shown that accelerating flow tends to delay transition to turbulence and decelerating flow tends to destabilize the flow and cause transition to turbulence.[23–25] Two dimensionless parameters that have been used to characterize regions of oscillating flow in pipes as fully laminar, fully turbulent, and laminar or turbulent over different parts of the oscillating flow cycle are Valensi number and maximum Reynolds number (see Ref. 26).

Figure 10 (see Ref. 27) characterizes laminar and turbulent regions of oscillating pipe flow. The region left of the transition lines is the region of always-laminar flow. As the angular frequency and, thus, the Valensi number increase, the always-laminar region extends over to the right to higher maximum Reynolds numbers. For the 1000-rpm modified CAST gas spring run discussed earlier, oscillating-flow Peclet number was about 3375. This corresponds to a Valensi number (oscillating-flow Peclet number/Prandtl number) of ~5000. Maximum Reynolds number, based on maximum piston velocity of ~4 m/s and maximum density of ~2.75 kg/m^3, was $\sim 2.3 \times 10^4$. This point is inside the always-laminar region. Of course, this is for pipe flow. The gas spring, with an oscillating piston inside a 5.1 cm (2-in.)- diam cylinder and with a maximum/minimum volume ratio of 2 might be more likely to experience turbulence at lower maximum Reynolds numbers.

Laminar Versus Turbulent Flow: Two-Space Test Rig

Rig operating conditions were 201.7 rpm and 1.008-MPa mean pressure. Maximum Reynolds numbers and Valensi numbers were calculated for the 34×20 grid, 120 time step/cycle simulation and compared with Fig. 10. It was found that the heat-exchanger maximum Reynolds number point ($Va = 7.8$, $Re_{\max} = 2370$) was in the neighborhood of the several transition lines between the always-laminar/sometimes-turbulent regions. This would imply that the heat-exchanger flow might be turbulent for part of the cycle. The cylinder maximum Reynolds number point ($Va = 420$, $Re_{\max} = 6300$) was in the always-laminar region. Measurements and analysis of oscillating pipe flow[25] have shown that flow may be turbulent and laminar over different parts of the same cycle; appropriate simulation involves switching back and forth between laminar and turbulent calculations. No data were available for the test rig to specify if and when the flow was turbulent. Therefore, runs made for comparison of laminar and turbulent flow used either the laminar or turbulent flow models over the entire cycle.

Conclusions

Fedorchenko's compressible nonacoustic equations[12] were used as a basis for modifying an existing incompressible two-dimensional code, CAST.[11] The resulting compressible nonacoustic two-dimensional code, modified CAST, was then used to model two reciprocating test rigs for which published data were available.[16–18] Modified CAST gas spring calculations agreed well with 10-rpm hysteresis loss data, ~50 and 500 rpm P–V diagram data, and also with compressible acoustic calculations of two-dimensional, 10-rpm gas spring, velocities and temperatures. However, modified CAST overpredicted two-space test-rig heat-exchanger heat fluxes, although trends were predicted well.

In general, acoustics will be unimportant inside reciprocating devices sufficiently small that acoustic-propagation times across the interiors are small compared to the cycle period. For the gas spring at 1000 rpm and the taller two-space test rig at ~200 rpm, simulated here, acoustic waves were calculated to travel across the maximum dimensions in less than 1.5% of the cycle period. Maximum Mach numbers for both test rigs were less than 0.01.

Fedorchenko's[12] compressible nonacoustic technique may have the capability for reductions in simulation time for specialized transient situations, for example, enclosed boundaries with time-varying volumes, where compressibility must be simulated but acoustics are not important.

References

[1]Ernst, W. D., and Shaltens, R. K., "Automotive Stirling Engine Development Project," NASA CR-190780, Feb. 1997.

[2]Dahr, M., "Stirling Space Engine Program," Vol. 1 Final Rept., NASA CR 19999-209164/VOL1, Aug. 1999.

[3]Tew, R. C., and Geng, S. M., "Overview of NASA Supported Stirling Thermodynamic Loss Research," NASA TM-105690, Aug. 1992.

[4]Thieme, L. G., Qiu, S., and White, M. A., "Technology Development for a Stirling Radioisotope Power System for Deep Space Missions," NASA TM-2000-209767, March 2000.

[5]Furlong, R., and Shaltens, R., "Technology Assessment of DOE's 55-We Stirling Technology Demonstrator Convertor (TDC)," NASA TM-2000-210509, Oct. 2000.

[6]Huang, S. C., "HFAST Version 2.0 Analysis Manual," NASA Contract Number NAS3-25330, NASA John H. Glenn Research Center at Lewis Field, Cleveland, OH, Jan. 1993.

[7]Gedeon, D., "Sage User's Guide," 3rd ed., Gedeon Associates, Athens, OH, 1999.

[8]Geng, S. M., and Tew, R. C., "Comparison of GLIMPS and HFAST Stirling Engine Code Predictions with Experimental Data," NASA TM-105549, Aug. 1992.

[9]Makhkamov, K., and Ingram, D. B., "Theoretical Investigations on the Stirling Engine Working Process," *Proceedings of 35th Intersociety Energy Conversion Engineering Conference*, AIAA, Las Vegas, NV, July 2000.

[10]Tew, R. C., Jr., "Two-Dimensional Compressible Non-Acoustic Modeling of Stirling Machine Type Components," Ph.D. Dissertation, Mech. Eng. Dept., Cleveland State Univ., Cleveland, OH, Dec. 2000.

[11]Peric, M., and Scheuerer, G., "CAST—A Finite Volume Method for Predicting Two-Dimensional Flow and Heat Transfer Phenomena," GRS—Technische Notiz SRR-89-01, Gesellschaft fur Reaktorsicherheit (GRS) mbh Forschungsgelande, 8046 Garching, Federal Republic of Germany, Sept. 1989.

[12]Fedorchenko, A. T., "A Model of Unsteady Subsonic Flow with Acoustics Excluded," *Journal of Fluid Mechanics*, Vol. 334, 1997, pp. 135–155.

[13]Ferziger, J. H., and Peric, M., *Computational Methods for Fluid Dynamics*, Springer-Verlag, Berlin, 1997, p. 327.

[14]Patankar, S. V., *Numerical Heat Transfer and Fluid Flow,* Hemisphere, Washington, DC, 1980, Chap. 6.

[15]Recktenwald, G. W., "A Study of Heat Transfer Between the Walls and Gas Inside the Cylinder of a Reciprocating Compressor," Ph.D. Dissertation, Mech. Eng. Dept., Univ. of Minnesota, 1989.

[16]Kornhauser, A. A., and Smith, J. L., Jr., "A Comparison of Cylinder Heat Transfer Expressions Based on Prediction of Gas Spring Hysteresis Loss," *Fluid Flow and Heat Transfer in Reciprocating Machinery*, edited by T. Morel, J. E. Dudenhoefer, T. Uzkan, and P. J. Singh FED-Vol. 62, HTD-Vol. 93, American Society of Mechanical Engineers, New York, Dec. 1987.

[17]Kornhauser, A. A., and Smith, J. L., Jr., "Heat Transfer During Compression and Expansion," Phase II Progress Report for Oak Ridge National Lab., Subcontract No. 19x-55915C, Cryogenic Engineering Lab., Dept. of Mechanical Engineering, Massachusetts Inst. of Technology, Cambridge, MA, 1988.

[18]Kornhauser, A. A., "Gas-Wall Heat Transfer During Compression and Expansion," Ph.D. Dissertation, Mech. Eng. Dept., Massachusetts Inst. of Technology, Cambridge, MA, 1989.

[19]Ibrahim, M. B., Tew, R. C., Zhang, Z., Gedeon, D., and Simon, T. W., "CFD Modeling of Free-Piston Stirling Engines," NASA TM 2001-211132, IECEC2001-CT-38, Sept. 2001.

[20]Morel, T., and Mansour, N. N., "Modeling of Turbulence in Internal Combustion Engines," Society of Automotive Engineers, SAE Paper 8200040, 1982.

[21]Launder, B. E., and Spalding, D. B., "The Numerical Computation of Turbulent Flows," *Computational Methods in Applied Mechanical Engineer*, Vol. 3, 1974, pp. 269–289.

[22]Koehler, W. J., Patankar, S. V., and Ibele, W. E., "Numerical Prediction of Turbulent Oscillating Flow and Associated Heat Transfer," NASA CR 197177, Aug. 1991.

[23]Seume, J., Friedman, G., and Simon, T. W., "Fluid Mechanics Experiments in Oscillatory Flow," NASA CR 189127, Vol. 1-Report, March 1992.

[24]Seume, J., Friedman, G., and Simon, T. W., "Fluid Mechanics Experiments in Oscillatory Flow," NASA CR 189128, Vol. 2-Tabulated Data, March 1992.

[25]Ibrahim, M., Bauer, C., Simon, T., and Qiu, S., "Modeling Oscillatory Laminar, Transitional, and Turbulent Channel Flows and Heat Transfer," *10th International Heat Transfer Conference*, Inst. of Chemical Engineer, Rugby, Warwickshire, UK, Aug. 1994.

[26]Simon, T. W., and Seume, J. R., "A Survey of Oscillating Flow in Stirling Engine Heat Exchangers," NASA CR 182108, March 1988.

[27]Ibrahim, M., and Kannapareddy, M., "Computational Heat Transfer Analysis for Oscillating Channel Flows," *First Indian Society of Heat and Mass Transfer (ISHMT)–American Society of Mechanical Engineers Heat and Mass Transfer Conference*, ISHMT, Bombay, India, Jan. 1994.